WAPD-T-3225

ASSESSMENT OF CRACKS IN STRESS CONCENTRATION REGIONS WITH LOCALIZED PLASTIC ZONES

E. Friedman

DE-AC11-93PN38195

BETTIS ATOMIC POWER LABORATORY WEST MIFFLIN, PENNSYLVANIA 15122-0079

Operated for the U.S. Department of Energy
by WESTINGHOUSE ELECTRIC COMPANY,
a division of CBS Corporation

(This Page Intentionally Blank)

DISCLAIMER

ASSESSMENT OF CRACKS IN STRESS CONCENTRATION REGIONS WITH LOCALIZED PLASTIC ZONES

E. Friedman

Westinghouse Electic Company
Bettis Atomic Power Laboratory
West Mifflin, PA

ABSTRACT

Many brittle fracture evaluation procedures include plasticity corrections to elastically computed stress intensity factors. These corrections, which are based on the existence of a plastic zone in the vicinity of the crack tip, can overestimate the plasticity effect for a crack embedded in a stress concentration region in which the elastically computed stress exceeds the yield strength of the material in a localized zone. The interactions between the crack, which acts to relieve the high stresses driving the crack, plasticity effects in the stress concentration region, and the nature and source of the loading are examined by formulating explicit flaw finite element models for a crack emanating from the root of a notch located in a panel subject to an applied tensile stress. The results of these calculations provide conditions under which a crack-tip plasticity correction based on the Irwin plastic zone size overestimates the plasticity effect. A failure assessment diagram (FAD) curve is used to characterize the effect of plasticity on the crack driving force and to define a less restrictive plasticity correction for cracks at notch roots when load-controlled boundary conditions are imposed. The explicit flaw finite element results also demonstrate that stress intensity factors associated with load-controlled boundary conditions, such as those inherent in the ASME Boiler and Pressure Vessel Code as well as in most handbooks of stress intensity factors, can be much higher than those associated with displacement-controlled conditions, such as those that produce residual or thermal stresses. Under certain conditions, the inclusion of plasticity effects for cracks loaded by displacement-controlled boundary conditions reduces the crack driving force thus justifying the elimination of a plasticity correction for such loadings. The results of this study form the basis for removing unnecessary conservatism from flaw evaluation procedures that utilize plasticity corrections.

INTRODUCTION

Brittle fracture evaluation procedures as given, for example, in Section XI of the ASME Boiler and Pressure Vessel Code (ASME, 1998) or the British Standard PD 6493, 1991 usually employ linear elastic stress intensity factor solutions for crack configurations in simple geometries to characterize the crack driving force for crack-like flaws located in regions of more complex geometry, such as stress concentration regions. In particular, the stress intensity factor solutions used for surface flaws are often those for surface cracks in finite thickness flat plates or in cylindrical shells subject to stresses applied on the crack face that are the same as the stresses at the crack location calculated in the absence of the crack. This approach is termed the implicit method, since the stress intensity factor is determined implicitly from (1) the stress distribution existing at the crack location but calculated in the absence of the crack, and (2) a stress intensity factor solution for a structure whose geometry may not resemble that of the region in which the crack is located; e.g., a stress concentration region such as a notch or a fillet radius. The stress intensity factor calculation, in effect, accounts directly for neither the geometry of the structure nor the source or nature of the loading that drives the crack. Explicit procedures such as energy release rate or domain integral methods that utilize finite element models with cracks included directly in the model accommodate the interaction of the crack, the component geometry, and the loading. This interaction can be especially important when distinguishing between cracks driven by primary loading, such as pressure, and secondary loading, such as thermal or residual stresses.

The effects of plasticity in flaw evaluation procedures are often expressed in terms of a plastic zone correction factor (see, for example, ASME, 1998) which is predicated on the assumption that the flaw is located in a region whose behavior is elastic if the flaw did not exist. Furthermore, in the presence of the crack-like flaw, the plasticity effect is simulated by a plastic zone existing in the vicinity of the crack tip. The size of the plastic zone is presumed to be small relative to the crack size or any other characteristic dimension. An effective crack size is then defined as the sum of the actual crack size and the distance from the crack tip to the center of the plastic zone (i.e., the plastic zone radius). For a material that does not strain harden, the plastic zone radius under these conditions is approximated by the distance ahead of

the crack tip in which the elastically calculated stress component acting normal to the crack surface exceeds the yield stress as described, for example, in Kanninen and Poplar (1985).

We consider here the case of a postulated flaw embedded in a stress concentration region in which the stresses calculated in the absence of the flaw exceed the yield stress of the material in a localized zone that under sufficiently high magnitudes of load may completely envelop the flaw. The localized plastic zone induced by a stress concentrator should be distinguished from the crack-tip plastic zone which is developed due to the presence of a crack in an otherwise elastic stress field. Two-dimensional elastic-plastic J integral calculations performed for cracks emanating from holes or other stress concentrators (see, for example, Sumpter and Turner (1976)) have shown that in some cases reasonably accurate J integral solutions can be estimated by calculating the elastic stress intensity factor with a crack-tip plastic zone correction and converting the calculated K to J even though the elastically calculated stresses exceed the yield stress. The presence of the crack in these cases relieves the stresses in the stress concentration region, thus focusing the plasticity at the crack tip. For the sufficiently shallow cracks considered in this paper, the plastic zone extends back to the free surface from which the crack emanates but does not extend across the uncracked ligament.

Explicit flaw finite element models provide a set of results for a relatively simple stress concentration region - a notched panel in tension - that under certain conditions can be used to support a less stringent plasticity correction for flaws embedded within a localized plastic zone induced by a stress concentration. Differences in the crack driving force resulting from secondary loading vice primary loading in cases where the implicit fracture evaluation procedure gives the same results for both types of loading are investigated using both elastic and elastic-plastic explicit flaw finite element models. The effects of plasticity and the conditions under which plasticity can either exacerbate or mitigate the crack driving force for displacement-controlled loading conditions are also examined.

EXPLICIT FLAW MODELING

The fracture evaluation of a relatively shallow surface crack emanating from a notch is a typical example of a fracture assessment of a crack in a stress concentration region for which plasticity ahead of the crack is contained by an outer elastic stress field. Figure 1 illustrates the notched panel and its dimensions. Two-dimensional elastic and elastic-plastic J integral calculations are performed for various size cracks under plane strain conditions using both an elastic energy release rate procedure for two-dimensional geometries and crack configurations and a domain integral approach for evaluating J integrals. Figure 2 is a contour plot of the elastically computed Mises equivalent stress in the uncracked panel subject to a remotely applied tensile stress of 20 ksi. This plot is superposed on the finite element mesh for a crack depth a = 0.3 inch and serves to illustrate the case of a flaw embedded in a localized plastic zone.

Elastic Energy Release Rate Calculations

The energy release rate algorithm described by Friedman (1984) calculates the change in potential energy of the structure as the crack extends by an amount equal to the length of a finite element. The decrease of potential energy normalized with respect to the amount of new crack face area created by the crack extension is equal to G, which is the same as the J integral for linear elastic materials. The crack is extended in a series of steps along a predefined path. The algorithm evaluates the potential energy change and the new crack area created for each crack extension and thus enables J to be determined as a function of crack size. J is converted to the stress intensity factor K_I for plane strain conditions by:

$$K_I = \sqrt{(EJ)/(1-\nu^2)} \qquad (1)$$

The energy release rate calculations determine the linear elastic K_I as a function of crack depth for load applied as a uniform tensile stress and for applied end displacements that give the same elastic stress distribution in the absence of the crack. (The implicit flaw procedures cited above give the same K_I solution for both of these cases.) Results are obtained for crack sizes up to 1 inch and panel heights H = 10, 20, 40, 100, and 400 inches. For load-controlled boundary conditions in which the loading is fixed at a prescribed value regardless of the crack size, the results are essentially independent of the panel height since the stresses in the vicinity of the crack are governed by the remotely applied load which does not vary with the panel height. Under displacement-controlled or "fixed grip" conditions, on the other hand, an increasing crack size results in a decreasing applied load in order to maintain the prescribed boundary displacements. The magnitude of the load under displacement-controlled conditions depends not only on the displacements but on the panel height. For increasingly larger panel heights, this load approaches that of the specified applied load (under load-controlled conditions) for relatively small crack sizes. Stress intensity factor solutions associated with load-controlled boundary conditions, however, always provide upper bounds to K_I values obtained using equivalent displacement boundary conditions.

Domain Integral Calculations

Under either linear elastic (LEFM) or elastic-plastic (EPFM) conditions, the domain integral algorithm in the ABAQUS (1994) finite element code calculates the J integral corresponding to a number of predefined paths in which the crack tip is enclosed. The J solution is theoretically path independent for linear or nonlinear elastic behavior; therefore, the degree of independence obtained from an analysis is a measure of the adequacy of the model. Explicit flaw models are established for three crack sizes: a = 0.1 inch (a/t = 0.033), a = 0.3 inch (a/t = 0.10), and a = 0.9 inch (a/t = 0.30), where t = 3 inches is the dimension of the uncracked ligament; and two panel heights: H = 10 inches and H = 100 inches. The finite element mesh consists of eight-node quadrilateral elements with reduced integration. The elements that focus at the crack tip (i.e., crack-tip elements) are also eight-node quadrilaterals which, in the undeformed configuration, are triangular. The nodes that converge at the crack tip are allowed to displace independently, and the midside nodes of the crack-tip elements are moved to the quarter-point positions in order to model, to some degree, the crack-tip singularities.

The finite element model defines seven paths over which the J integral is calculated. The average of the J values from six of these paths is computed (the J integral for the path closest to the crack tip is excluded) and then converted to an equivalent K_I using Eq. (1). Values of K_I computed in this way are valid stress intensity factors only under linear elastic fracture mechanics conditions for which yielding is con-

fined to the crack tip region. Nevertheless, all J results are converted to K_I in order to compare results from various analyses.

J integral values are determined assuming both linear elastic and nonlinear elastic-plastic material behavior for the three crack sizes. In all cases, the panel is loaded by specifying as boundary conditions a uniform tensile stress at the panel ends (load-controlled) or a set of end displacements identical to the displacements obtained from a linear elastic analysis of the panel loaded by the uniform tensile stress in the absence of the crack (displacement-controlled). Under elastic conditions, the stress distribution in the uncracked panel is the same for the two cases, and the stress intensity factors calculated using an implicit flaw method which uses the stresses at the crack location regardless of their source are also the same. The elastic properties of the material used in the analyses are: $E = 30 \times 10^6$ psi, $\nu = 0.3$. Plasticity effects are expressed in the form of a stress vs. plastic strain relationship characterized by the Ramberg-Osgood power law:

$$\varepsilon_{pl}/\varepsilon_{ys} = \alpha(\sigma/\sigma_{ys})^n \qquad (2)$$

where σ_{ys} is the yield stress, $\varepsilon_{ys} = \sigma_{ys}/E$, and α and n are fitting parameters. In the absence of well-established stress vs. strain curves, approximate values of α and n are used for both A508, Cl. 2 low-alloy pressure vessel steel and the higher strength A508, Cl. 4 steel which exhibits less strain hardening. This enables a comparison of plasticity effects for the two materials. Values of σ_{ys}, α, and n are 50 ksi, 2.144, and 6.03, respectively, for A508, Cl. 2 and 85 ksi, 1.620, and 9.88 for A508, Cl. 4 at 70°F. The deformation plasticity mechanical behavior model is used in ABAQUS to generate J integral solutions accommodating plasticity effects. In all cases, the J integral values calculated from the six integration paths do not vary by more than 0.2 percent.

ASME CODE PLASTICITY CORRECTION TO ELASTIC STRESS INTENSITY FACTOR SOLUTION

In the implicit flaw evaluation procedure described in A-3000 of Appendix A to Section XI of the ASME Code (ASME, 1998), stress intensity factors are determined by first performing a linear elastic calculation without the flaw included in the model. For the notched panel under an applied tensile load, the resulting stresses σ_{yy}, acting normal to the crack surface at the crack location y=0 are used to calculate the stress intensity factor. The plasticity corrected stress intensity factor is based on the Appendix A crack-tip plastic zone correction which is embodied in the K_I solution as follows:

$$K_I = \sigma_{eq}\sqrt{\frac{\pi a}{Q}} \qquad (3)$$

where $Q = \xi_2^2 - (1/6)(\sigma_{eq}/\sigma_{ys})^2$. ξ_2 is the complete elliptic integral of the second kind and is a function of the crack aspect ratio *a/l* (for the two-dimensional model under consideration, $\xi_2 = 1$); σ_{eq} is the equivalent crack opening stress which is a function of stress coefficients and stress correction factors, which in turn depend on whether a linear or a cubic polynomial stress fit is used. The corresponding elastic solution K_{Ie}, is given by the same expression with the plastic zone correction removed; thus, ξ_2^2 replaces Q in Eq. (3). Q is then expressed in terms of K_{Ie} as:

$$Q = \xi_2^2\left[1 - \frac{1}{6\pi a}\left(\frac{K_{Ie}}{\sigma_{ys}}\right)^2\right] \quad , \qquad (4)$$

which gives the following for K_I as a function of K_{Ie}:

$$K_I = \frac{K_{Ie}}{\left[1 - \frac{1}{6\pi a}\left(\frac{K_{Ie}}{\sigma_{ys}}\right)^2\right]^{0.5}} \quad . \qquad (5)$$

This expression corresponds to a plastic zone size $a_{pzc} = (K_I/\sigma_{ys})^2/6\pi$. Note that the plastic zone corrected K_I is indeterminate if the elastically computed $K_{Ie} \geq \sigma_{ys}\sqrt{6\pi a}$. Consistent with the plastic zone correction, elastically computed stress intensity factors determined from explicit rather than implicit flaw models can be corrected for plastic zone effects using Eq. (5).

RESULTS OF CALCULATIONS

Elasticity and deformation theory plasticity calculations are performed to determine (1) the effect of the source of the loading on the crack driving force, (2) the adequacy of the plastic zone correction, and (3) the interaction between the source of the loading and the plasticity effects.

Elastic Stress Intensity Factors for Applied Tensile Stress and Equivalent Boundary Displacement Loadings

The results of elastic energy release rate calculations demonstrate the effect of the nature and source of the loading on the crack driving force. Stress intensity factor solutions are obtained for crack depths up to 0.9 inch. The applied loading conditions are a uniform tensile stress of 20 ksi and prescribed sets of boundary displacements that, in the absence of the crack, result in the same stress distribution as that developed by the applied tensile stress . (These loading conditions yield the same stress intensity factor solutions in accordance with the implicit flaw fracture evaluation procedure.) The displacement boundary condition case is applied for a wide range of panel heights in order to ascertain the relative degree of conservatism that exists in the implicit flaw procedure when no distinction is made between displacement-controlled and load-controlled conditions.

Figure 3 shows plots of the elastic stress intensity factor K_I, against the crack depth a, for an applied tensile stresses of 20 ksi. (Stress intensity factor plots for other magnitudes of applied tensile stress would be similar since the elastic K_I is proportional to the applied load.) Curves for displacement-controlled boundary conditions given for panel heights ranging from 10 inches to 400 inches show that although the crack driving force under displacement-controlled conditions is less than that under load-controlled conditions, the mitigation of K_I depends very much on the panel height. The effect of panel height on the K_I solution can be explained in terms of the effect of the crack on the compliance of the structure. Under linear elastic conditions, the presence of a crack enhances the compliance of the structure. For displacement-controlled conditions, the added compliance due to the presence of the crack becomes more significant relative to the compliance of the uncracked panel as the height of the panel decreases. This is an inverse spring effect since, for a very large panel height, the

uncracked structure is very compliant. Under displacement-controlled or "fixed grip" conditions, an increase in the compliance decreases the stored energy that is available to drive the crack. Therefore, the increase in the compliance relative to that of the uncracked structure results in a decreased stress intensity factor. For relatively shallow cracks, the added compliance is small regardless of the panel height and the differences between the stress intensity factor solutions for load-controlled boundary conditions and those for the various displacement-controlled boundary condition cases are inconsequential, as shown in Figure 3. For increasingly deeper cracks, however, the compliance effect results in an increasing mitigation of the crack driving force. Hence, the combined effects of the increasing crack size and the decreasing panel height act to enhance the effect of the compliance change in decreasing the stress intensity factor, as also illustrated in Figure 3. For extremely large panel heights, the added compliance due to the presence of the crack is insignificant relative to the compliance of the entire structure regardless of the crack depth; in this case, the stress intensity factors using displacement-controlled boundary conditions approach those for load-controlled conditions.

The crack driving stresses developed by the displacement boundary conditions are akin to the thermal stresses that would be generated by a temperature decrease in a similar panel that is constrained against displacement at some distance h, from the crack. The results plotted in Figure 3 demonstrate the importance of the location of the defect relative to the constraints that are imposed to assure displacement compatibility for a thermally loaded structure. Such constraints generate secondary stresses due to thermal loading as well as to weld-induced shrinkage.

Figure 3 also shows a plot of K_I vs. a obtained using the implicit flaw procedure with no crack-tip plastic zone correction. The stress intensity factors from the implicit flaw procedure agree reasonably well with those from the explicit flaw analysis provided the prescribed boundary condition for the latter is the applied tensile stress. The implicit flaw K_I solutions, however, can be much higher than those calculated under displacement-controlled conditions which exist if the crack is being driven, for example, by thermal or residual stresses.

Plasticity Effects for Applied Tensile Stress Loading

Elastic and deformation theory plasticity calculations are conducted using ABAQUS explicit flaw models for specified applied tensile stresses (load-controlled boundary conditions) to assess the implicit flaw procedure plasticity correction for cracks embedded completely within a localized plastic zone induced by a stress concentrator as well as for cracks penetrating the plastic zone into elastic material. Since applied loads produce higher crack driving forces than equivalent boundary displacements, this set of calculations is conducted for the bounding or most limiting case. As will be shown later, the effect of plasticity on the crack driving force is also maximized for this case. J integrals are computed for crack sizes of 0.1, 0.3, and 0.9 inch, and for applied tensile stresses ranging from 5 ksi to 50 ksi. The results are independent of panel height since the boundary conditions are load-controlled.

Plasticity effects are characterized by making use of the failure assessment diagram (FAD) concept as described, for example, by Hong et al. (1994) to assess flaws in a stress concentration region. In the FAD approach, the effect of plasticity on the crack driving force is graphically depicted by the construction of a curve of K_r vs. S_r, where $K_r = \sqrt{J_e/J}$ and $S_r = \sigma_{appl}/\sigma_{lim}$. J_e and J are the elastically calculated J integral and the J integral calculated including plasticity effects, respectively, while σ_{appl} and σ_{lim} are the applied tensile stress and the limit load stress of the uncracked ligament, respectively. K_r is an inverse measure of plasticity since lower values of K_r indicate an enhanced plasticity effect. K_r associated with the crack-tip plastic zone correction is given by $K_r = K_{Ie}/K_I$, where K_I is determined as a function of K_{Ie} from Eq. (5). This gives:

$$K_r = \left[1 - (K_{Ie}/\sigma_{ys})^2/(6\pi)\right]^{0.5} \tag{6}$$

S_r, on the other hand, is a dimensionless measure of the magnitude of the applied load. The limit load membrane stress σ_{lim}, which is obtained from the Kumar et al. (1981) plane strain limit load solution for an edge-cracked plate in tension, is given by:

$$\sigma_{lim} = 1.455\left\{\left[1 - 2\left(\frac{a}{t}\right) + 2\left(\frac{a}{t}\right)^2\right]^{0.5} - \frac{a}{t}\right\}\sigma_{ys} \tag{7}$$

The quantity "a" in Eq. (7) represents the depth of the edge crack which, for the notched panel, is the sum of the notch depth (2 inches) and the depth of the crack emanating from the notch root. The thickness t, is the total width of the panel which in this case is 5 inches. Eq. (7) applies to material that does not strain harden. The actual limit load will be somewhat greater as a result of strain hardening. Note that σ_{lim} in this case is used as a normalizing parameter.

FAD curves obtained using load-controlled applied tensile stress boundary conditions are plotted in Figures 4 and 5 for A508, Cl. 2 and Cl. 4 steels, respectively. Each figure shows curves plotted for three crack depths (depth of crack emanating from the notch root): 0.1 inch, 0.3 inch, 0.9 inch. They correspond to plasticity corrections determined both from elastic and deformation plasticity explicit flaw finite element results and from the implicit flaw procedure crack-tip plastic zone correction, as given by Eq. (6), applied to the elastic finite element results. Note that the latter set of curves (K_r vs. S_r) is independent of σ_{ys} and, therefore, is the same for both materials.

Figures 4 and 5 show that for all load levels the magnitude of the crack-tip plastic zone correction for the bounding load-controlled conditions is much greater than that of the plasticity correction obtained using explicit flaw finite element J integral results for the relatively shallow cracks with depths a = 0.1 inch and a = 0.3 inch. These cracks are completely embedded in a plastic zone when S_r values exceed 0.351 and 0.590, respectively, for these two depths. The plasticity correction, therefore, is overestimated for these crack sizes regardless of whether the cracks are completely embedded in the plastic zone induced by the stress concentration or they penetrate the plastic zone into elastic material. For the crack with depth a = 0.9 inch, on the other hand, the crack-tip plastic zone correction is somewhat less than the explicit flaw correction for the range of S_r values shown on these figures. This relatively deep crack, however, penetrates beyond the plastic zone up to an applied stress level corresponding to an S_r value of 2.205. The trends of the a = 0.9 inch curves in Figs. 4 and 5 indicate that the curves will cross well short of S_r = 2.205. Hence, for loads high enough that the 0.9 inch crack is completely embedded in a plastic zone, the magnitude of the crack-tip plastic zone correction will be greater than that of the explicit flaw finite element correction. These

results indicate: (1) a reduction in the plasticity correction is justified for cracks of any size provided they are embedded within a localized zone of plasticity induced by a stress concentration, and (2) the plasticity correction can be mitigated for cracks that penetrate the plastic zone produced by the stress concentration if the crack depth is sufficiently small.

Although Figs. 4 and 5 show that shallower cracks produce a higher plasticity correction in terms of the FAD characterization, the FAD curves for both A508, Cl. 2 and Cl. 4 do not vary significantly with either the crack depth or the material for the notched panel. This suggests the possible definition of a bounding FAD curve to characterize the plasticity correction for cracks embedded in a plastic zone and for cracks penetrating the plastic zone into elastic material provided they are sufficiently shallow. Crack size criteria would need to be developed to implement the latter.

Interaction Between Plasticity Effects and Type of Loading

The interaction between plasticity effects and the nature of the applied loading (load-controlled vs. displacement-controlled) is illustrated by obtaining linear elastic J integral results and deformation plasticity J solutions for an applied tensile stress of 20 ksi and for three crack sizes (a = 0.1, 0.3, 0.9 inch) and two panel heights (H = 10, 100 inches). The deformation plasticity calculations use tensile properties characteristic of both A508, Cl. 2 and A508, Cl. 4. The explicit flaw J integral solutions are converted to K_I using Eq. (1).

The equivalent K_I solutions for panel heights of 10 inches and 100 inches are plotted in Figures 6 and 7, respectively. They show that plasticity effects are much smaller for displacement-controlled conditions (open symbols in Figures 6 and 7) than for load-controlled conditions (closed symbols). Figure 6 indicates that under displacement-controlled conditions, plasticity effects tend to decrease the crack driving force for the 10 inch panel height, while Figure 6 shows the opposite effect for the 100 inch panel height. Hence, the size of the constrained region (i.e., the distance from the constraint to the defect location), which is a direct measure of the compliance of the uncracked structure, determines whether plasticity effects are beneficial or detrimental for this type of loading. This may be explained by noting that the intensity of the plastic strain concentration at the crack location increases when the ratio of the compliance of the panel to the added compliance due to the presence of the crack increases. (This is often referred to as the "elastic follow-up" effect.) Although the plasticity effects are qualitatively different for these two panel heights, Figures 6 and 7 show that they are quantitatively small compared to the plasticity effects for equivalent load-controlled conditions. These figures also show that the elastic stress intensity factor solutions calculated under load-controlled boundary conditions provide upper bounds to the equivalent K_I solutions for displacement-controlled conditions in all cases except those for which the panel height is very large and the crack depth is relatively small. This corresponds to the high elastic follow-up case for which the compliance ratio is quite high and the plastic strain concentration, therefore, is quite intense. Figure 7 for the 100 inch panel height shows that for sufficiently small cracks, the elastic follow-up is sufficient to cause the equivalent K_I calculated for displacement-controlled conditions to exceed the elastically calculated stress intensity factor for load-controlled conditions. These results, therefore, support a conclusion that for structures stressed as a result of constraints necessary to assure displacement compatibility, a plasticity correction to the stress intensity factor calculated using load-controlled boundary conditions can be conservatively neglected unless the imposed constraint is far enough away from the crack location that the compliance ratio defined above is too high.

CONCLUSIONS

Explicit flaw finite element calculations for a notched panel in tension with cracks located in regions of localized plasticity lead to the following conclusions:

1. The crack-tip plastic zone correction in implicit flaw fracture evaluation procedures can overestimate plasticity effects in localized stress concentration regions in which the elastically computed stresses exceed the material yield strength. This results from stress intensity factor solutions that are based on the elevated stresses in the stress concentration region containing the crack, but that do not account directly for the geometry of the region, the presence of a zone of localized plasticity induced by the stress concentrator, nor the nature and source of the loading.

2. For load-controlled boundary conditions, whose plasticity effects conservatively bound those associated with displacement-controlled conditions, the crack-tip plastic zone correction overpredicts the plasticity effect for cracks completely embedded within a localized plastic zone.

3. The crack-tip plasticity correction also overestimates the plasticity effect for cracks that penetrate the plastic zone induced by the stress concentrator into elastic material provided the crack is sufficiently shallow.

4. A generalized plasticity correction to an elastically computed stress intensity factor solution can be characterized by a failure assessment diagram (FAD) curve, which graphically depicts the plasticity effect as a function of the applied load. For load-controlled conditions, which maximize the plasticity effects, the enhancement of the crack driving force due to plasticity varies significantly with neither the crack depth nor the material tensile properties. This suggests the possibility of defining a bounding plastic zone correction for cracks embedded in a localized plastic zone in terms of a bounding FAD curve.

5. Implicit flaw stress intensity factor evaluation procedures utilize the stress distribution at the crack location calculated in the absence of the crack regardless of the source of the stresses. They do not distinguish between primary stresses driven by load-controlled boundary conditions, such as pressure, and secondary stresses that are essentially displacement-controlled, such as residual or thermal stresses. Explicit flaw finite element analyses demonstrate that elastic stress intensity factors calculated using displacement-controlled boundary conditions are lower than those determined from load-controlled conditions that give the same stresses in the absence of the crack. The differences between the two solutions are small for very shallow cracks, but increase with increasing crack depth.

6. The degree of conservatism of the implicit procedure, which is based on stress intensity factor solutions associated with load-controlled boundary conditions, varies inversely with the size of the region that is constrained when the procedure is applied to conditions for which stresses are developed as a result of constraints on deformation. For relatively small constrained regions, such as might be expected when dealing with weld-induced residual stresses, stress intensity fac-

tors calculated using solutions for load-controlled conditions can be much too high. If, on the other hand, the constraint against deformation is acting at a considerable distance from the crack location, as might be expected in many cases of thermal loading, the degree of conservatism is much less.

7. Plasticity effects are small for displacement-controlled conditions compared with those for load-controlled conditions. The plasticity effect for the former tends to decrease the crack driving force unless the region that is being constrained is very large in which case the intensity of the strain concentration at the root of the notch is exacerbated and the plasticity increases the crack driving force. Hence, the size of the constrained region determines whether plastic zone effects are beneficial or detrimental. For sufficiently small cracks, moreover, the stress intensity factor can even exceed the elastically calculated K_I for equivalent load-controlled conditions.

8. Under load-controlled conditions, for which plasticity effects are more pronounced than for displacement-controlled conditions, the effect of plasticity on the crack driving force increases with increasing crack depth.

9. The plasticity effect is greater for A508, Cl. 2 steel than for A508, Cl. 4 for a given crack size. This is due to the different yield strengths and strain hardening characteristics of the two materials. The higher yield strength of A508, Cl. 4 produces a smaller region of plasticity under specified loading conditions. This is consistent with the crack-tip plastic zone correction formulation. Characterization of the plasticity effect in terms of the FAD curve, however, accommodates the different yield strengths and thus allows the possibility of the correction to be expressed in terms of a single FAD curve applicable to both materials.

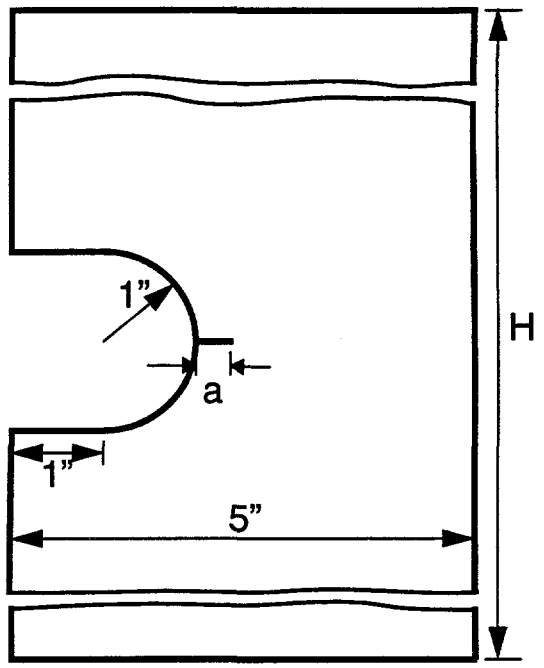

Figure 1. Notched Panel Geometry

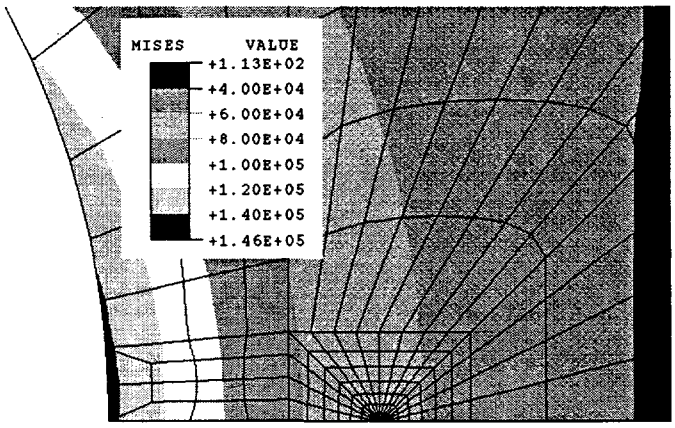

Figure 2. Contour Plot of Mises Equivalent Stress in Uncracked Panel for Applied Tensile Stress of 20 ksi

REFERENCES

ABAQUS/Standard User's Manual,, 1994, Version 5.4, Hibbitt, Karlsson & Sorensen, Inc., Pawtucket, RI.

ASME Boiler & Pressure Vessel Code, 1998, Section XI, Rules for Inservice Inspection of Nuclear Power Plant Components, Appendix A, pp. 401-422.

Friedman, E., 1984, "Curvature Effects in Thick Cylindrical Shells With Continuous Surface Cracks," Proceedings, Fifth International Conference on Pressure Vessel Technology - Vol. II: Materials and Manufacturing, ASME, New York, pp. 761-776..

Hong, Q., Ying, T., and Liankui, S., 1994, "The Assessment of Flaws in a High Stress Concentration Region," Intl. J. Pres. Ves. & Piping, Vol. 57, pp. 201-206.

Kanninen, M. F., and C. H. Popelar, C. H., 1985, Advanced Fracture Mechanics, Oxford University Press, New York, p. 172.

Kumar, V., German, M. D., and Shih, C. F., 1981, "An Engineering Approach for Elastic-Plastic Fracture Analysis," EPRI NP-1931, Project 1237-1, General Electric Co., Schenectady, NY.

PD 6493, 1991, Guidance on Methods for Assessing the Acceptability of Flaws in Fusion Welded Structures, British Standards Institution, London.

Sumpter, J. D. G., and Turner, C. E., 1976, "Design Using Elastic-Plastic Fracture Mechanics," Intl. J. Fracture, Vol. 12, No. 6, pp. 861-871.

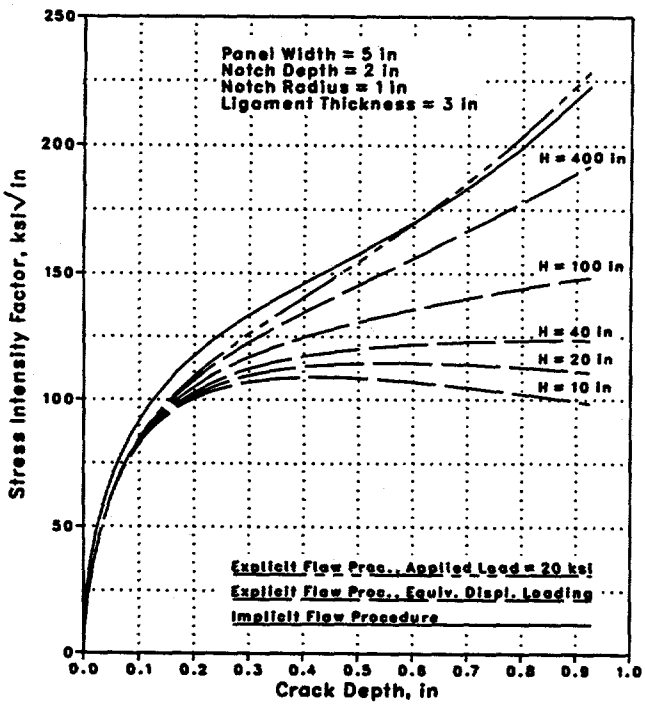

Figure 3. Elastic Stress Intensity Factor vs. Crack Depth for Notched Panel Under Applied Tensile Stress of 20 ksi

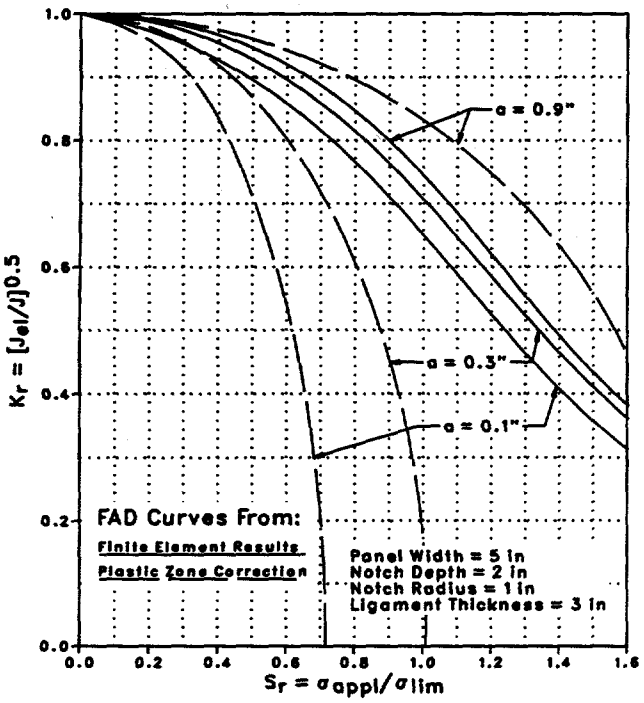

Figure 4. FAD Curve Plasticity Corrections for A508, Cl. 2 Notched Panel

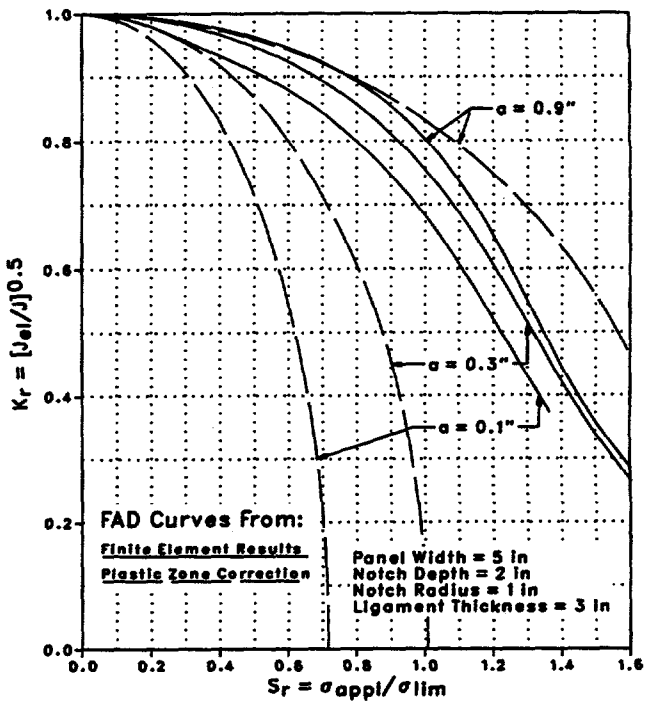

Figure 5. FAD Curve Plasticity Corrections for A508, Cl. 4 Notched Panel

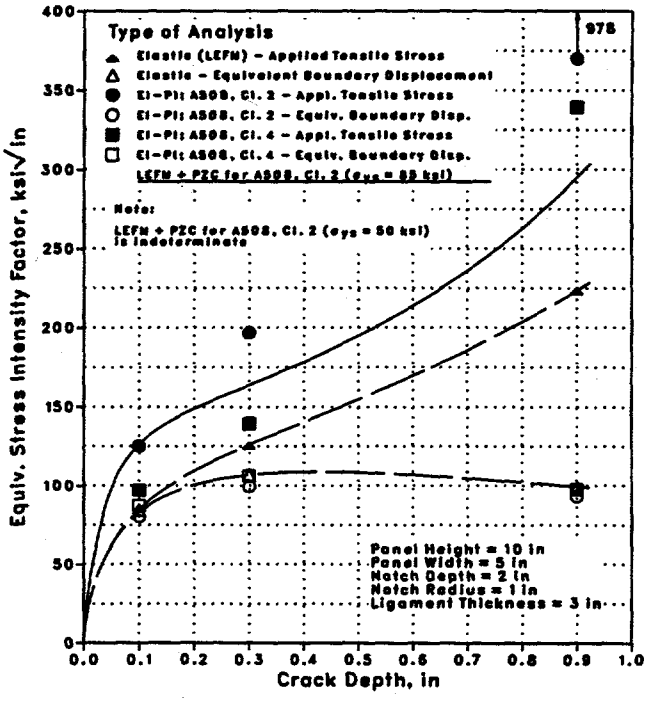

Figure 6. Equivalent Stress Intensity Factor vs. Crack Depth for 10 inch Notched Panel Under Applied Tensile Stress of 20 ksi

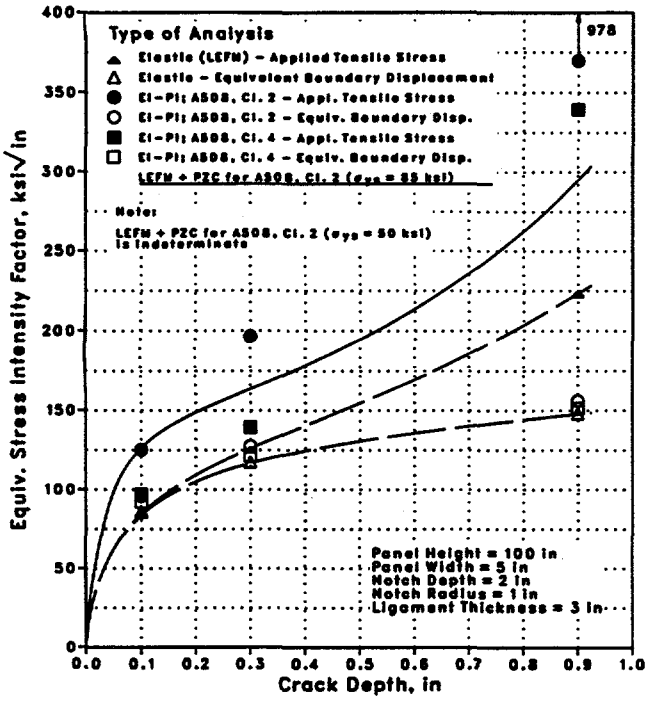

Figure 7. Equivalent Stress Intensity Factor vs. Crack Depth for 100 inch Notched Panel Under Applied Tensile Stress of 20 ksi